Jamming and percolation in random sequential adsorption of extended objects on a triangular lattice with quenched impurities

Jamming and percolation in random sequential adsorption of extended objects on a triangular lattice with quenched impurities

Lj Budinski-Petković[1], I Lončarević[1], Z M Jakšić[2] and S B Vrhovac[2,3]

[1] Faculty of Engineering, Trg D. Obradovića 6, Novi Sad 21000, Serbia
[2] Institute of Physics Belgrade, University of Belgrade, Pregrevica 118, Belgrade 11080, Serbia

E-mail: vrhovac@ipb.ac.rs

Abstract. Random sequential adsorption (RSA) on a triangular lattice with defects is studied by Monte Carlo simulations. The lattice is initially randomly covered by point-like impurities at a certain concentration p. The deposited objects are formed by self-avoiding random walks on the lattice. Jamming coverage θ_{jam} and percolation threshold θ_{p}^* are determined for a wide range of impurity concentrations p for various object shapes. Rapidity of the approach to the jamming state is found to be independent on the impurity concentration. The jamming coverage θ_{jam} decreases with the impurity concentration p and this decrease is more prominent for objects of larger size. For a certain defect concentration, decrease of the jamming coverage with the length of the walk ℓ making the object is found to obey an exponential law, $\theta_{\mathrm{jam}} = \theta_0 + \theta_1 \mathrm{e}^{-\ell/r}$. The results for RSA of polydisperse mixtures of objects of various sizes suggest that, in the presence of impurities, partial jamming coverage of small objects can have even larger values than in the case of an ideal lattice. Percolation in the presence of impurities is also studied and it is found that the percolation threshold θ_{p}^* is practically insensitive to the concentration of point defects p.

[3] http://ipb.ac.rs/vrhovac/

Percolation can be reached at highest impurity concentrations with angled objects, and the critical defect concentration p_c is lowest for the most compact objects.

Keywords: classical Monte Carlo simulations, percolation problems (theory)

Contents

1. Introduction

Adsorption of particles on various substrates is a phenomenon which underlies a number of processes of great technological, environmental and biological importance. For example, it is crucial for the separation of mixtures, filtration, catalysis, and protein adsorption in living cells. A number of adsorption processes of large particles, where events occur essentially irreversibly on the time scales of interest, can be studied as random sequential adsorption (RSA). In RSA processes particles are randomly, sequentially and irreversibly deposited onto a substrate. The particles are not allowed to overlap and they are permanently fixed at their spatial positions, so each adsorbed particle affects the geometry of all later placements. Thus, the dominant effect in RSA is the blocking of the available substrate area and the limiting (jamming) coverage θ_{jam} is less than in close packing. The kinetic properties of a deposition process are described by the time evolution of the coverage $\theta(t)$, which is the fraction of the substrate area occupied by the adsorbed particles. For a review of RSA models see [1–4].

Depending on the system of interest, the substrate can be continuum or discrete and RSA models can differ in substrate dimensionality. Exact solutions of RSA models are available only for deposition of k-mers on a one-dimensional lattice [5, 6] and for quasi-one-dimensional systems [7, 8]. On the other hand, for two-dimensional deposition problems Monte Carlo simulations remain one of the primary investigating tools [9–18].

Approach to the jamming coverage is known to be algebraic for continuum systems [9–12] and exponential for lattice models [13–18]. In the latter case the late-time kinetics of the process is described by the time dependence:

$$\theta(t) = \theta_{\text{jam}} - A\mathrm{e}^{-t/\tau}, \tag{1}$$

where A and τ are the parameters that depend on the details of the model, such as shape and orientational freedom of deposited objects. It was shown [16] that the rapidity of the approach is determined by the symmetry properties of deposited objects.

Polydispersity is a common feature of real physical systems. Irreversible deposition of mixtures has been studied for the case of binary mixtures [19–21], mixtures obeying various distributions [22, 23], and for multicomponent mixtures on discrete substrates [17]. Results of the simulations [19] indicate that the mixtures cover the lattice more efficiently than either of the species separately, and that the kinetics of the process depends on the symmetry properties of deposited objects [21]. In the case of polydisperse mixtures [17], where the number of components is gradually increased by adding objects of larger size, a strong dependence of the jamming limit of n-component mixtures on the shape of the adsorbed objects is observed. For the mixtures of more symmetric shapes jamming coverage increases with n, while for the less symmetric (angled) shapes jamming coverage decreases with addition of larger objects to the mixture.

During the process of irreversible deposition the number of deposited objects increases, causing the growth of clusters of occupied sites. Percolation assumes the existence of a large cluster that reaches two opposite sides of the substrate [24]. Formation of long-range connectivity in disordered systems is of great importance [25] in many physical, chemical and even sociological systems [26]. The problem of percolation attracts considerable interest [27–37] thanks to its applications in numerous practical problems such as conductivity in composite materials, flow through porous media, polymerization, and behavior of scale-free random networks such as the internet [38].

The temperature behavior of the percolation threshold of a system of adsorbed flexible chains was studied in [29], motivated by irreversible deposition of large particles, such as polymers and nanoparticles. The flexibility of chains was controlled by the temperature via the Boltzmann factor. The impact of the composition of flexible chains on percolation properties was discussed in [30] for square and for triangular lattice. Simulations were performed for various chain lengths and the most favorable compositions (for which the percolation threshold acquires its minimal values) were identified. For longer and more bent chains a no-percolating regime was detected. The interplay between RSA and percolation has been discussed in several works [20, 27, 28, 39, 40]. In [40] the results for the percolation thresholds, jamming coverages and their ratios were given for the deposition of various objects on a triangular lattice. Deposited objects were positioned by directed self-avoiding walks on the lattice. It was found that for elongated shapes the percolation threshold monotonically decreases, while for more compact shapes it monotonically increases with the object size. For various objects of the same length, the percolation threshold of more compact objects exceeds that of the elongated ones. However, for larger sizes of compact objects such as triangles and hexagons, a no-percolation regime was observed. The absence of percolation has also been reported in the studies of RSA of large rectangular particles [41], squares [42], and bent particles [30] on a square lattice.

The impact of defects on the percolation of k-mers on a square lattice is studied in [43–45]. In [45] two models are analyzed—in the first it is assumed that some fraction of sites is initially occupied by nonconducting point defects, and in the second that some fraction of the sites in the k-mers is nonconducting. The dependence of the percolation threshold on the length of the k-mers and on the impurity concentration is analyzed. Above some critical concentration of defects, percolation is blocked even at the jamming limit.

Here we present the results of extensive simulations of irreversible deposition of objects of various shapes on a triangular lattice initially covered with point impurities at various concentrations. The deposited objects are positioned by self-avoiding random walks on the lattice. Jamming coverages and percolation thresholds are determined for a wide range of impurity concentrations. In order to gain an insight into the effect of defects on the adsorption phenomena in complex systems, simulations are also performed for mixtures made of various objects differing in shape and size.

Section 2 describes the details of the simulations. The results of the simulations for random sequential adsorption of various objects on a triangular lattice with various impurity concentrations are given in section 3, and the results for percolation on a triangular lattice with defects are given in section 4. Finally, section 5 contains some additional comments and final remarks.

2. Definition of the model and the simulation method

In our model the substrate is a triangular lattice initially occupied by nonconducting point defects at concentration p. The coverage of interest is due only to the extended objects. The deposited objects are positioned by self-avoiding random walks of length ℓ. Special attention has been paid to the deposition of basic shapes shown in table 1: k-mers, angled objects and triangles. Objects of larger sizes are made by repeating each step of a basic shape the same number of times. Exception is made for triangles, where larger objects also occupy all comprised sites. The construction of larger objects is illustrated in tables 2–4.

The Monte Carlo simulations are performed on a triangular lattice of linear size up to $L = 500$ sites. For the approach to the jamming coverage, periodic boundary conditions are used in all directions. On the other hand, when studying percolation, hard boundary conditions are used in the horizontal direction, in which the onset of percolation is detected, and periodic boundary conditions in the other two directions.

At each Monte Carlo step a lattice site is selected at random. If the selected site is unoccupied, deposition of the object is tried in one of the six orientations. We fix the beginning of the walk that makes the shape at the selected site and search whether all successive ℓ sites are unoccupied. If so, we occupy these $\ell + 1$ sites and place the object. If the attempt fails, a new site and a new direction are selected at random. The jamming limit is reached when no more objects can be placed in any position on the lattice. In the case of mixtures, deposition of one of the objects making the mixture is selected with equal probability at each Monte Carlo step. The time is counted by the number

Table 1. Construction of basic shapes (x) of various symmetry orders $n_s^{(x)}$.

(x)	Shape	$n_s^{(x)}$	$\ell^{(x)}$
(A)	⊢•	2	1
(B)	•—•—•	2	
(C)	⌐/	1	2
(D)	⌐\	3	

Table 2. Jamming coverages θ_{jam} for various impurity concentrations p, percolation thresholds θ_{p}^* for $p = 5\%$, and critical impurity concentrations p_c for line segments of different lengths ℓ.

Shape		θ_{jam}				θ_{p}^*	p_c
		$p = 0\%$	$p = 10\%$	$p = 20\%$	$p = 50\%$		
⊢•	$\ell = 1$	0.9194(5)	0.8142(6)	0.7139(6)	0.4131(6)	0.4832(7)	42.93(8)
•—•—•	$\ell = 2$	0.8358(7)	0.7179(5)	0.6064(6)	0.2957(6)	0.4603(8)	33.62(7)
...	$\ell = 3$	0.7888(7)	0.6494(7)	0.5248(7)	0.2081(8)	0.4385(9)	27.41(7)
...	$\ell = 4$	0.7579(6)	0.5956(6)	0.4593(7)	0.1433(7)	0.4261(9)	22.81(6)
...	$\ell = 5$	0.7356(8)	0.5501(7)	0.4036(7)	0.0954(8)	0.4175(8)	19.06(8)
...	$\ell = 6$	0.7212(7)	0.5115(8)	0.3565(7)	0.0615(8)	0.4103(9)	16.54(6)
...	$\ell = 7$	0.7089(8)	0.4769(7)	0.3154(7)	0.0387(8)	0.4098(9)	13.91(6)
...	$\ell = 8$	0.6985(8)	0.4472(9)	0.2784(9)	0.0224(8)	0.4071(10)	11.49(8)
...	$\ell = 9$	0.6906(9)	0.4175(7)	0.2468(8)	0.0138(8)	0.4047(12)	10.68(9)
...	$\ell = 10$	0.6847(8)	0.3918(9)	0.2209(9)	0.0074(9)	0.4003(10)	8.27(9)

Note: The numbers in parentheses are the numerical values of the standard uncertainty of $\theta_{\text{jam}}^{(x)}$, θ_{p}^*, and p_c referred to the last digits of the quoted value.

Table 3. Jamming coverages θ_{jam} for various impurity concentrations p, percolation thresholds θ_{p}^* for $p = 5\%$, and critical impurity concentrations p_c for angled objects of different lengths ℓ.

Shape		θ_{jam}				θ_{p}^*	p_c
		$p = 0\%$	$p = 10\%$	$p = 20\%$	$p = 50\%$		
⌐/	$\ell = 2$	0.8345(6)	0.7364(6)	0.6373(7)	0.3383(6)	0.4574(9)	37.95(8)
⌐_/	$\ell = 4$	0.7184(6)	0.6057(7)	0.4996(7)	0.1985(5)	0.4060(9)	29.10(7)
...	$\ell = 6$	0.6502(7)	0.5178(8)	0.4039(7)	0.1085(7)	0.3781(11)	22.35(8)
...	$\ell = 8$	0.6039(8)	0.4520(7)	0.3327(7)	0.0522(8)	0.3561(12)	17.94(8)
...	$\ell = 10$	0.5689(8)	0.4019(8)	0.2773(8)	0.0218(9)	0.3405(10)	14.56(9)
...	$\ell = 12$	0.5458(8)	0.3608(9)	0.2344(8)	0.0077(9)	0.3262(12)	12.44(8)
...	$\ell = 14$	0.5230(7)	0.3254(8)	0.1976(8)	0.0024(8)	0.3195(10)	10.43(9)
...	$\ell = 16$	0.5059(9)	0.2951(9)	0.1686(8)	0.0007(9)	0.3146(11)	8.85(7)
...	$\ell = 18$	0.4915(9)	0.2702(8)	0.1416(9)	0.0002(9)	0.3056(11)	7.97(9)
...	$\ell = 20$	0.4777(9)	0.2462(9)	0.1219(9)	0.00005(9)	0.2986(10)	7.16(8)

Note: The numbers in parentheses are the numerical values of the standard uncertainty of $\theta_{\text{jam}}^{(x)}$, θ_{p}^*, and p_c referred to the last digits of the quoted value.

Table 4. Jamming coverages θ_{jam} for various impurity concentrations, percolation thresholds θ_{p}^* for $p = 5\%$, and critical impurity concentrations p_c for triangles of different lengths ℓ.

| Shape		θ_{jam}				θ_{p}^*	p_c
		$p = 0\%$	$p = 10\%$	$p = 20\%$	$p = 50\%$		
	$\ell = 2$	0.7971(4)	0.6864(4)	0.5775(4)	0.2598(5)	0.5222(9)	25.16(6)
	$\ell = 5$	0.7206(5)	0.5746(5)	0.4326(6)	0.0871(5)	0.5498(9)	11.77(6)
...	$\ell = 9$	0.6814(6)	0.4885(6)	0.3111(5)	0.0135(6)	0.5759(10)	5.49(7)
...	$\ell = 14$	0.6572(7)	0.4124(6)	0.1998(6)	0.0006(6)	0.6020(9)	2.28(7)
...	$\ell = 20$	0.6406(7)	0.3381(8)	0.1059(7)	0.00003(7)	/	0.58(7)

Note: The numbers in parentheses are the numerical values of the standard uncertainty of $\theta_{\text{jam}}^{(x)}$, θ_{p}^*, and p_c referred to the last digits of the quoted value.

of attempts to select a lattice site and scaled by the total number of lattice sites. In all the simulations the data are averaged over 1000 independent runs.

The impact of defects on percolation is also studied. The coverage of the surface is increased in the RSA process up to the percolation threshold, when a cluster appears that extends through the whole system—from the left to the right side of the lattice. The tree-based union/find algorithm was used to determine the percolation threshold [46, 47]. Each cluster of connected sites is stored as a separate tree, having a single 'root' site. All sites of the cluster possess pointers to the root site, so it is simple to ascertain whether two sites are members of the same cluster. When a deposited object connects two separate clusters, they are amalgamated by adding a pointer from the root of the smaller cluster to the root of the larger one. This procedure is repeated until the percolation threshold is reached, i.e. until the opposite sides of the lattice are connected by a single cluster.

3. Impact of defects on the RSA on a triangular lattice

For all the examined object shapes simulations are performed for a wide range of impurity concentrations. The approach to the jamming coverage is examined for objects covering three lattice sites—line segments, angled objects and triangles, shown in table 1 as objects B, C and D. For each shape three example results for the time dependence of $\ln(\theta_{\text{jam}} - \theta(t))$ are shown in figure 1. The plots are obtained both for the ideal lattice and the lattice covered by impurities of concentrations $p = 10\%$ and $p = 20\%$. We can see that for the late stages of the process the plots are mutually parallel straight lines for each shape, suggesting that the rapidity of the approach to the jammed state is not affected by the presence of impurities. The values of the parameter τ obtained from the slopes of the lines depend on the order of the symmetry axis of the shape: $\tau \simeq 6$ for shapes with a symmetry axis of first order, $\tau \simeq 3$ for shapes with a symmetry axis of second order, and $\tau \simeq 2$ for shapes with a symmetry axis of third order. Towards the
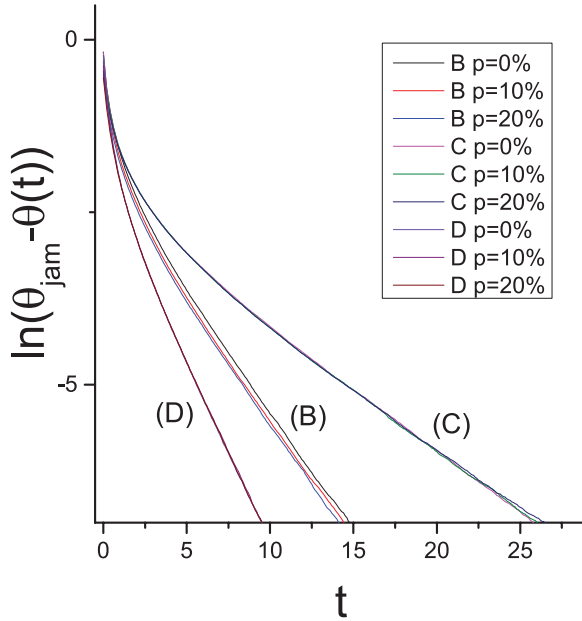
Figure 1. Plots of $\ln(\theta_{\mathrm{jam}} - \theta(t))$ versus t for objects B, C, and D for various impurity concentrations, as indicated in the legend.

end of the process objects of higher order of symmetry can fill the isolated empty locations in more different orientations and the relaxation time decreases with the order of symmetry axis.

The dependence of the jamming coverage θ_{jam} on the impurity concentration p is shown in figure 2 for various sizes $\ell = 1, 2, 3, \ldots$ of k-mers, angled objects and triangles. The corresponding jamming densities θ_{jam} are also given in tables 2–4. The size of the object ℓ is determined by the length of the walk that makes the shape. The whole range of impurity concentrations from $p = 0$ to 95% is examined. In addition, in figure 3 we show the typical snapshots of the jammed-state configurations obtained for objects of length $\ell = 10$ and different impurity concentrations p. As expected, jamming coverage θ_{jam} of the deposited objects decreases with the concentration of impurities and this decrease is more prominent for larger objects. The decrease of the jamming coverage θ_{jam} is almost linear up to very high impurity concentrations for the smallest objects of each shape, while the adsorption of larger objects is more affected by the presence of impurities.

Figure 4 shows the dependence of the jamming coverage θ_{jam} on the length of the walks ℓ placing the objects for various impurity concentrations p for (a) k-mers, (b) angled objects and (c) triangles. The lines represent the exponential fit of the form:

$$\theta_{\mathrm{jam}} = \theta_0 + \theta_1 \mathrm{e}^{-\ell/r}, \tag{2}$$

where θ_0, θ_1 and r are parameters that depend on the concentration of impurities p and on the object shape. The values of the parameter r versus impurity concentration p are presented in figure 4(d) for the three objects examined. It can be seen that the parameter r increases with p for low impurity concentrations, reaches a maximum, and decreases for higher values of p. The decrease of the jamming coverage with ℓ is slowest for $p \simeq 10$–15%, while for lower and higher values of impurity concentrations p the curves show sharper dependence on ℓ.
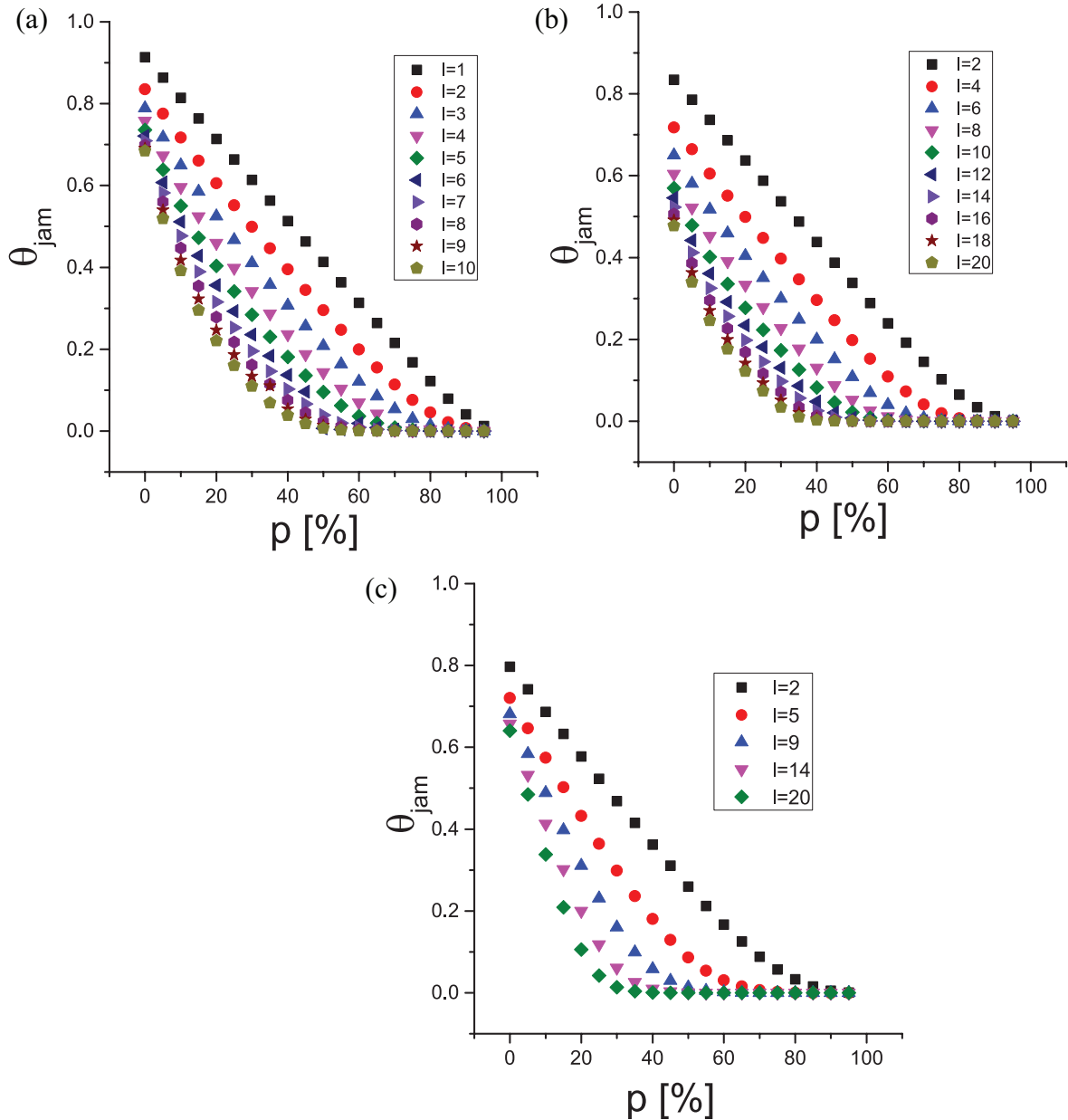
Figure 2. Jamming coverages θ_{jam} versus impurity concentration p for: (a) k-mers, (b) angled objects, and (c) triangles made by walks of various lengths ℓ, as indicated in the legend.

Jamming coverage θ_{jam} for three different objects covering the same number of sites is given as a function of impurity concentration p in figure 5. Objects B, C and D from table 1 show similar dependence of the jamming coverage on the impurity concentration. Jamming coverage of the angled objects displays a slightly higher resistance to the increase of defect concentration p than the jamming coverage of the other two objects. This is due to their enhanced ability for avoiding the sites with defects. Indeed, if we compare the jamming state snapshots in figure 3, it is clearly evident that the jamming coverage of the linear objects is more affected by the increase of impurity concentration from $p = 10\%$ to $p = 20\%$ than the jamming coverage of the angled objects. A mixture
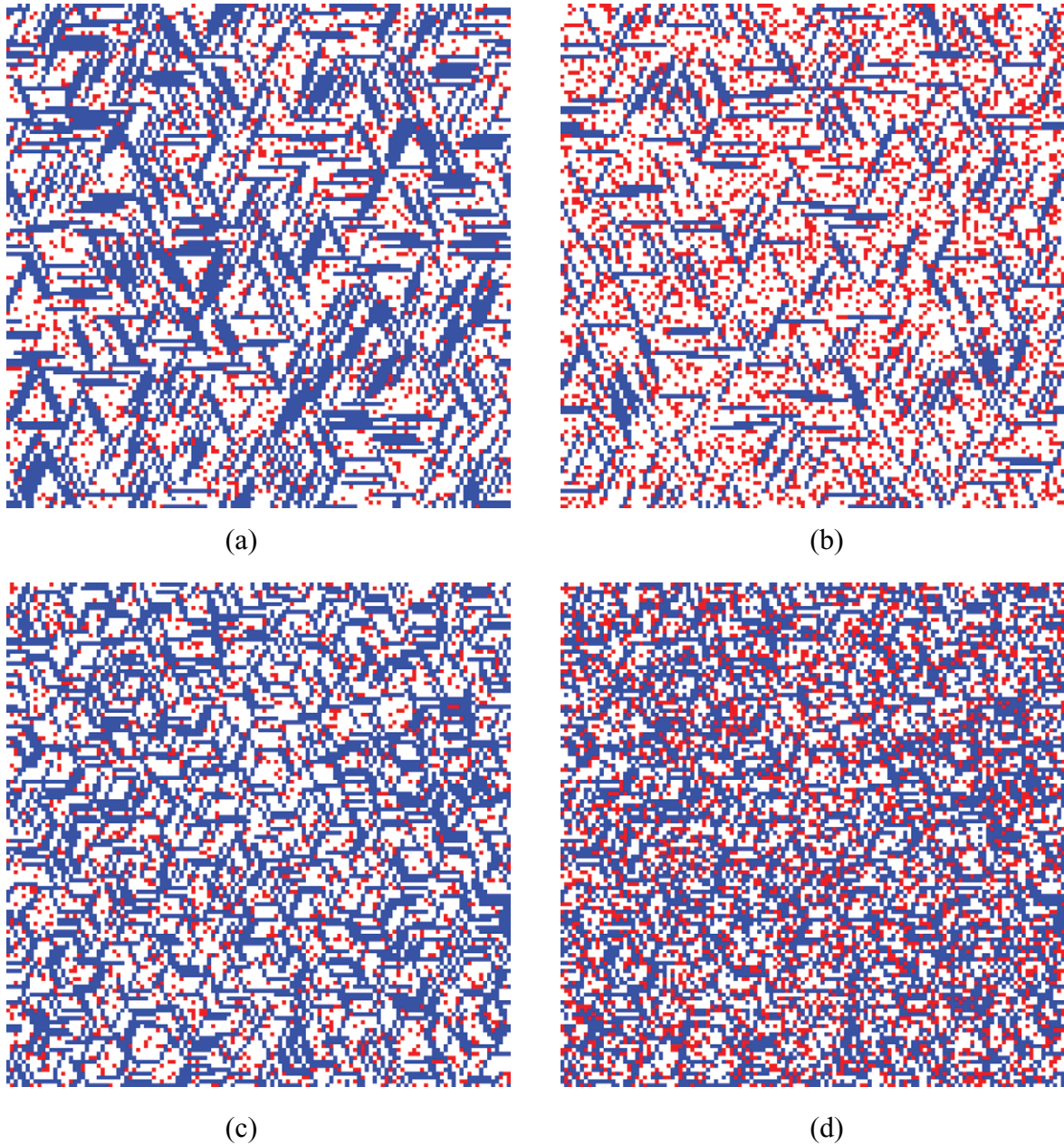
Figure 3. Typical jamming configurations obtained for objects covering ten lattice sites ($\ell = 9$) and different impurity concentrations p: (a) line segments, $p = 10\%$; (b) line segments, $p = 20\%$; (c) angled objects, $p = 10\%$; and (d) angled objects, $p = 20\%$. Deposited objects and point defects are colored in blue and red, respectively. Empty nodes are white.

of these three objects is also examined and the results for the partial jamming coverages are presented in figure 6. Here the differences due to the object shape are more prominent. In the competition between the adsorption of these three objects, the object with greater probability for avoiding the sites with impurities wins more often. This is the reason why the adsorption of the angled object is most favorable, and the adsorption of triangles, as compact objects, is suppressed when depositing from the mixture.
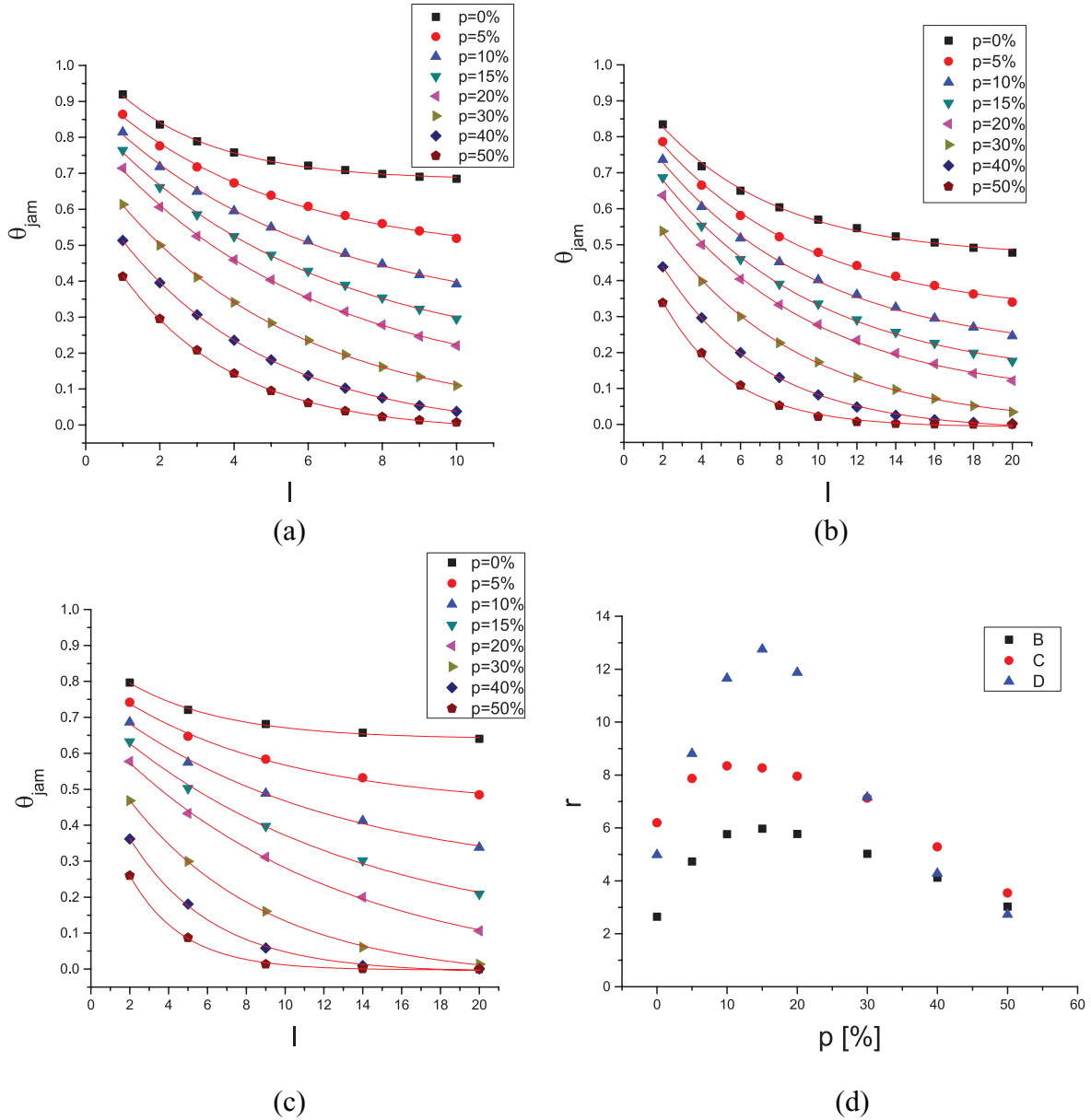
Figure 4. Dependence of the jamming coverage θ_{jam} on the length of the walk ℓ positioning k-mers (a), angled objects (b), and triangles (c), for various impurity concentrations p. The lines represent the exponential fit of the form (2). Plot (d) illustrates the dependence of the parameter r from exponential fit (2) on the impurity concentration p.

Mixtures of objects of the same shape but various sizes are also studied. Ten-component mixtures are made of line segments and also of angled objects of various lengths, while a mixture of triangles contains five objects of various sizes. Figure 7 gives partial jamming coverages for these three mixtures as a function of the impurity concentration p. For the sake of clarity, only the results for the five smallest objects making each mixture are presented. It is interesting to emphasize that the dependence of the partial jamming coverage is a nonmonotonic function of the impurity concentration
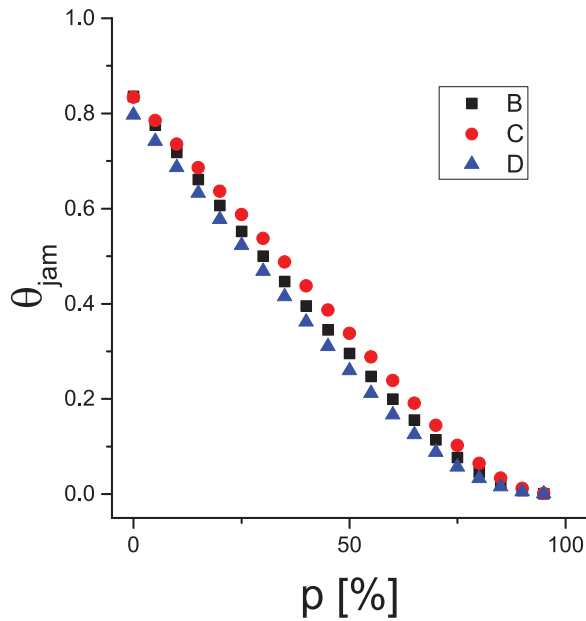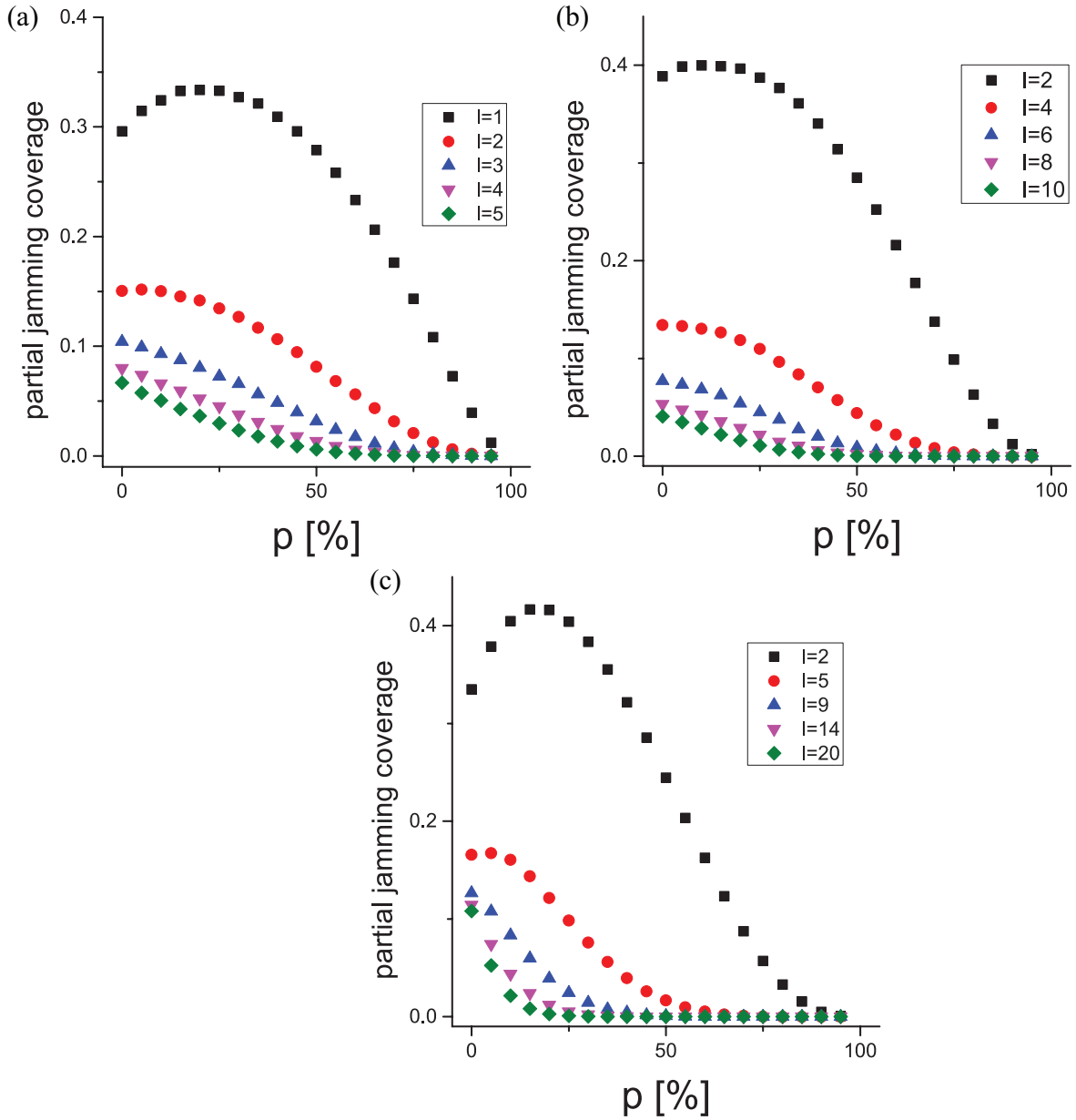
Figure 5. Jamming coverages θ_{jam} versus impurity concentration p for objects B, C and D (see table 1).
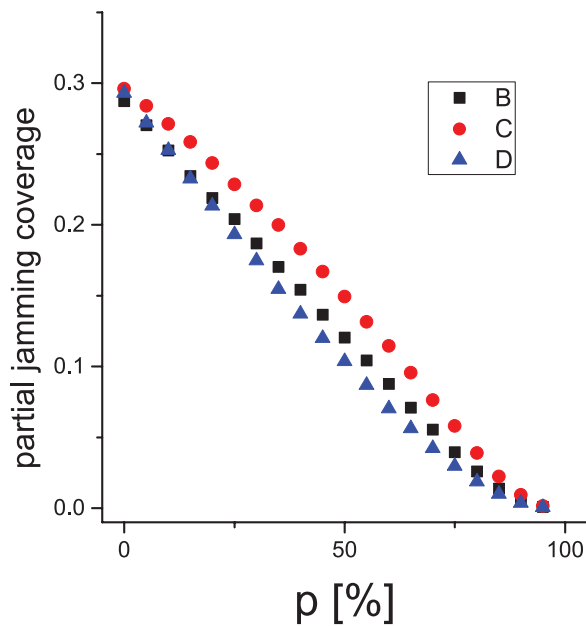
Figure 6. Partial jamming coverages versus impurity concentration p for the mixture of objects B, C and D (see table 1).

p for small objects of length $\ell = 1$ and $\ell = 2$. It grows with p for low impurity concentrations, reaches a maximum, and decreases for larger concentrations of defects. This is most obvious for the case of dimers and for the smallest triangles. Adsorption of smaller objects is favored in the presence of defects, and at relatively low impurity concentrations the coverage due to small objects can have even higher values than in the case of an ideal lattice.

Figure 7. Partial jamming coverages versus impurity concentration p for various lengths of the walks ℓ placing the objects for the (a) ten-component mixture of k-mers, (b) ten-component mixture of angled objects, and (c) five-component mixture of triangles. Only the results for the five smallest objects making each mixture are presented.

4. Percolation in the presence of impurities

For percolation-type systems, it is known [24] that the finite scaling theory correctly describes the dependence of the effective percolation threshold θ_{p} (the mean value of threshold measured for a finite lattice), and its standard deviation σ on the linear size L of the lattice. In such systems one assumes that the effective percolation threshold θ_{p} approaches the asymptotic value $\theta_{\mathrm{p}} \to \theta_{\mathrm{p}}^{*}$ $(L \to \infty)$ via the power law:
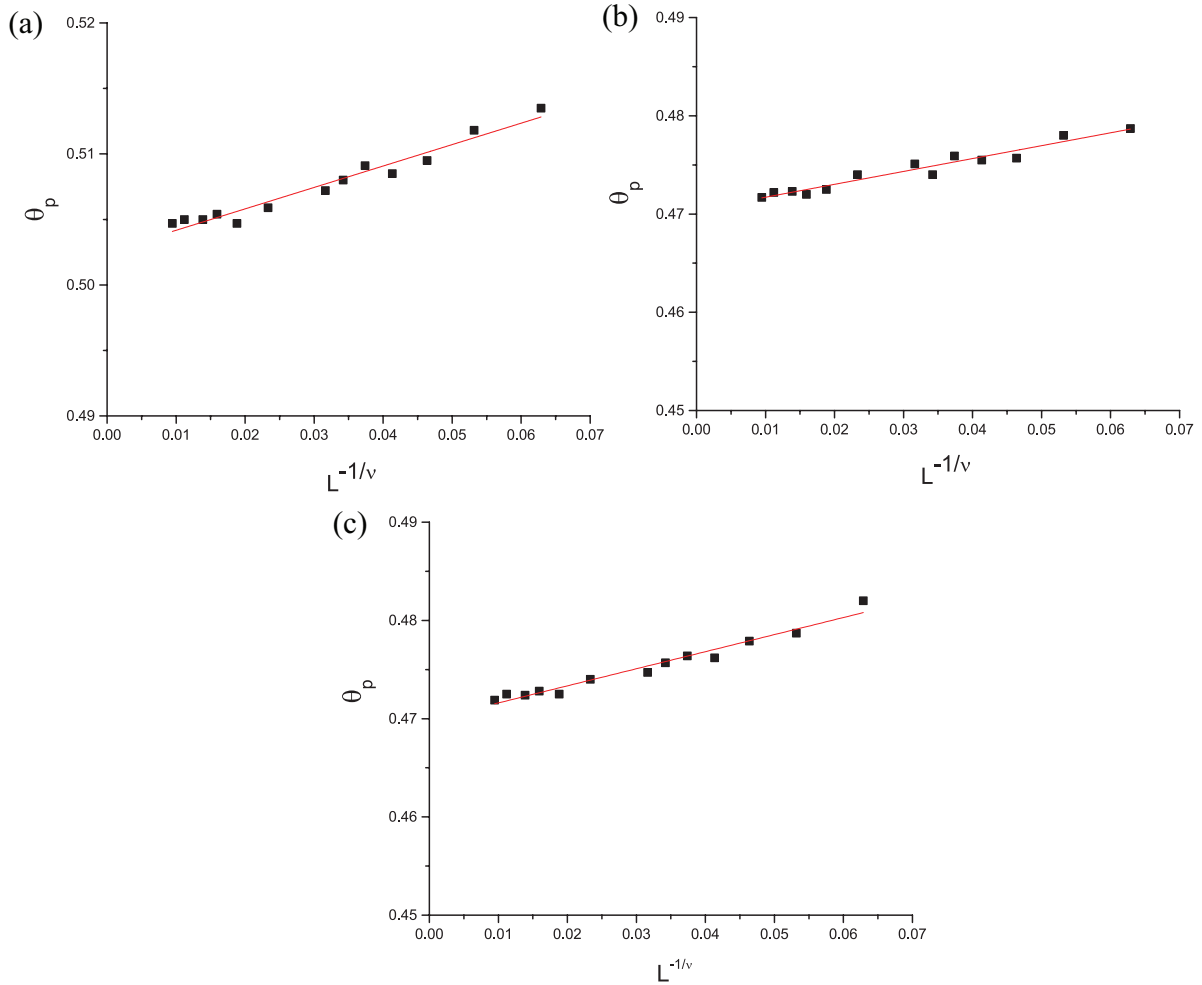
Figure 8. Finite-size scaling of the percolation threshold θ_p against $L^{-1/\nu}$ with $\nu = 4/3$ for objects (a) B, (b) C, and (c) D for impurity concentration $p = 10\%$.

$$\theta_p - \theta_p^* \propto L^{-1/\nu} \; . \tag{3}$$

Here θ_p^* is the exact percolation threshold (as $L \to \infty$) and the constant ν is the critical exponent that governs the divergence of the correlation length as $\xi \propto |\theta_p - \theta_p^*|^{-\nu}$. For 2D systems the theoretical value for the correlation length exponent is $\nu = 4/3$ [24]. Relationship (3) allows us to extrapolate the threshold for an infinite lattice, $L \to \infty$.

Simulations were performed for lattices of various sizes ranging from $L = 30$ to $L = 500$ for smaller objects and from $L = 100$ to $L = 1000$ for the largest ones. Plotting the mean value of the threshold θ_p for various lattice sizes against $L^{-1/\nu}$, we confirm the validity of the finite-size scaling in the system and determine the asymptotic value of the percolation threshold. In figure 8 finite-size scaling is illustrated for objects covering three lattice sites—line segments, angled objects and triangles, for impurity concentration $p = 10\%$.

In addition, it appears from the scaling theory that the standard deviation σ of the percolation threshold measured for a finite lattice vanishes as a power of the system size L:
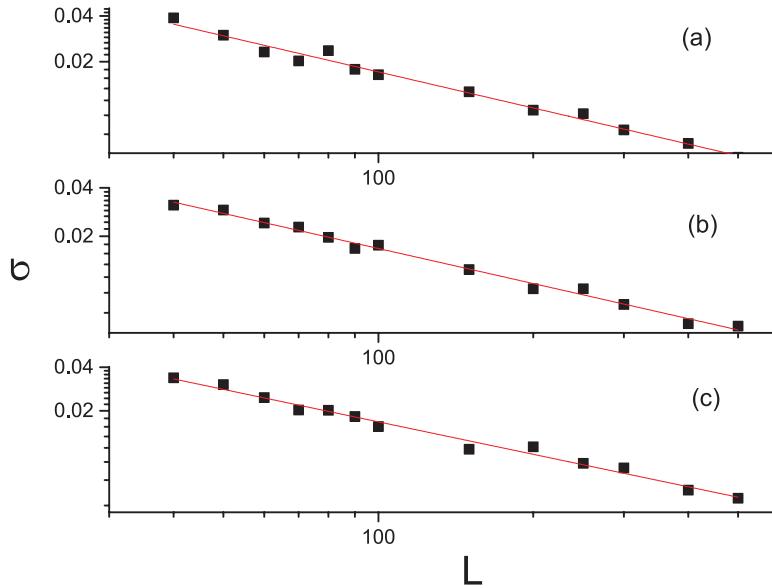
Figure 9. Standard deviations σ of the percolation threshold on a double logarithmic scale for: (a) trimer (B), (b) angled object (C), and (c) triangle (D) for impurity concentration $p = 10\%$. Straight lines correspond to the best fit according to the power law of equation (4) and with the exponents 0.77 ± 0.03, 0.73 ± 0.02 and 0.74 ± 0.03 for objects (B), (C), and (D), respectively.

$$\sigma \propto L^{-1/\nu} \ . \tag{4}$$

The above relationship (4) allows us to measure the critical exponent ν. As expected, the exponent value has been found to be $1/\nu = 0.75 \pm 0.05$, compatible with $1/\nu = 3/4$ value known for 2D percolation. Indeed, in figure 9 the standard deviation σ versus L is shown on a double logarithmic scale for (a) trimer (B), (b) angled object (C), and (c) triangle (D) for impurity concentration $p = 10\%$. For all objects and impurity concentrations we obtained confirmation of the power law of equation (4) with the value of the exponent $1/\nu$ ranging from 0.73 ± 0.02 to 0.77 ± 0.03. Therefore, these results are in good agreement with the universal value $1/\nu = 3/4$.

Percolation thresholds θ_p^* are determined for various sizes ℓ of the basic objects B, C and D for a wide range of impurity concentrations p. While the jamming coverage θ_{jam} decreases as the concentration of defects p grows, the percolation threshold θ_p^* is found to be practically insensitive to the point-like defect concentration. It seems that the possibility of forming a percolating cluster depends only on the coverage of the lattice, regardless of the presence of impurities. Consequently, the values of the percolation threshold θ_p^* for all objects in the case of $p = 5\%$ are given in tables 2–4. The values of θ_p^* in the case of the lattice without impurities ($p = 0$) are given elsewhere [40]. The percolation threshold θ_p^* and the jamming coverage θ_{jam}, as well as their ratio θ_p^*/θ_{jam}, are plotted against the length ℓ of the line segments in figure 10(a) for the lattice without impurities ($p = 0$) and in figures 10(b) and (c) for impurity concentrations $p = 5\%$ and $p = 10\%$ respectively. The jamming coverage θ_{jam} monotonically decreases with ℓ, while the percolation threshold θ_p^* decreases for shorter line segments, reaches a value
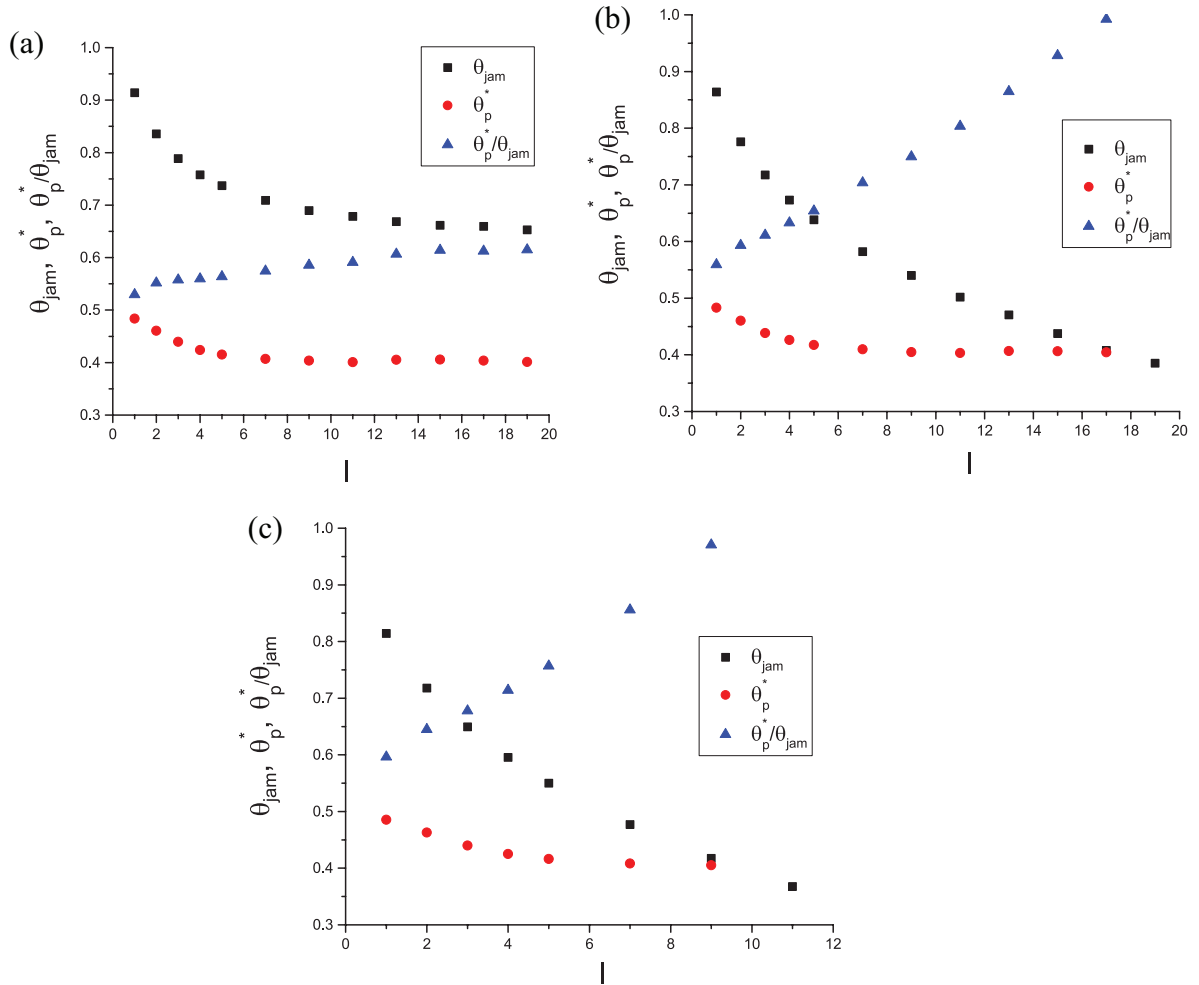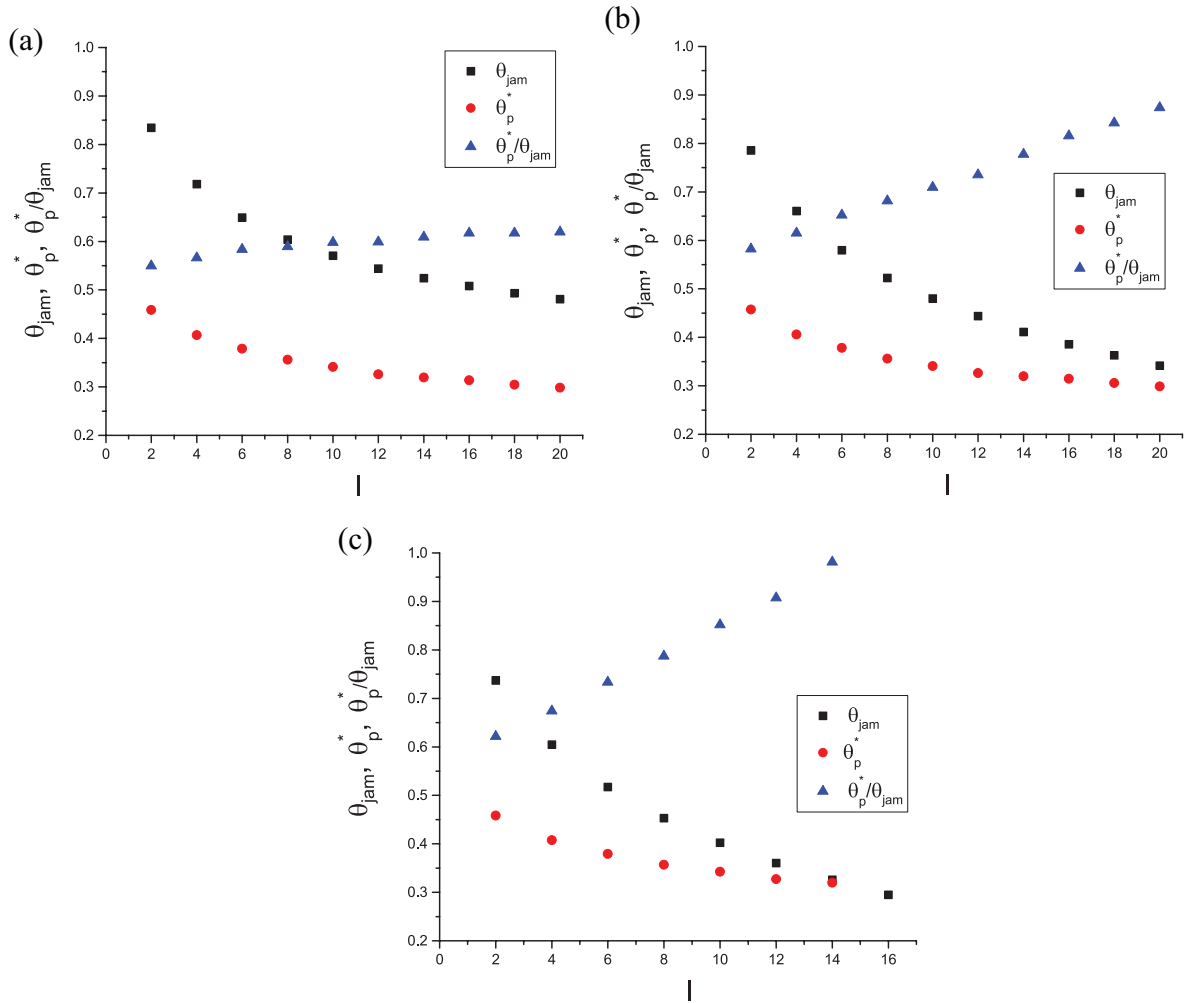
Figure 10. Dependence of the jamming coverage θ_{jam}, the percolation threshold θ_{p}^*, and the ratio $\theta_{\text{p}}^*/\theta_{\text{jam}}$ on the length of k-mers ($k = \ell + 1$) for three different concentrations of impurities: (a) $p = 0\%$, (b) $p = 5\%$, and (c) $p = 10\%$.

$\theta_{\text{p}}^* \simeq 0.401$ for $\ell = 11$, and it seems that θ_{p}^* does not significantly depend on ℓ for longer k-mers. Consequently, the ratio $\theta_{\text{p}}^*/\theta_{\text{jam}}$ increases. Since the jamming coverage decreases with the impurity concentration p, ratio $\theta_{\text{p}}/\theta_{\text{jam}}$ increases more sharply for higher defect concentrations, as can be seen from figures 10(b) and (c). In figure 10(b) the last point is missing since percolation is not reached for the line segments covering 20 lattice sites. For the lattice covered with impurities at concentration $p = 10\%$, percolation cannot be reached for line segments covering more than ten lattice sites, so in figure 10(c) results are not shown for longer objects.

The results for the percolation threshold θ_{p}^*, the jamming coverage θ_{jam}, and their ratio $\theta_{\text{p}}^*/\theta_{\text{jam}}$ are shown in figure 11 for the angled objects of various lengths ℓ. Percolation threshold θ_{p}^* and the jamming coverage θ_{jam} are monotonically decreasing functions of the object length ℓ in the presence of impurities, as well as for the initially clean lattice. Their ratio $\theta_{\text{p}}^*/\theta_{\text{jam}}$ increases with ℓ, but for the lattice without defects this increase slows down with ℓ and becomes more prominent when the
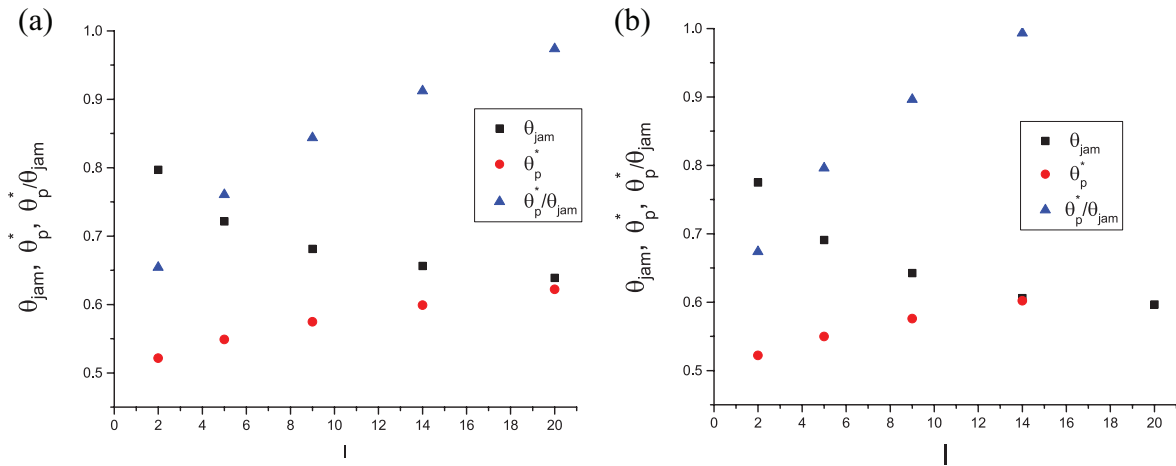
(a)

(b)

(c)

Figure 11. Dependence of the jamming coverage θ_{jam}, the percolation threshold θ_{p}^*, and the ratio $\theta_{\text{p}}^*/\theta_{\text{jam}}$ on the length ℓ of angled objects for three different concentrations of impurities: (a) $p = 0\%$, (b) $p = 5\%$, and (c) $p = 10\%$.

impurity concentration p increases. From figure 11(c) we can see that at impurity concentration $p = 10\%$ percolation cannot be reached by angled objects covering more than 15 lattice sites.

In the case of triangles the jamming coverage θ_{jam} decreases, but the percolation threshold θ_{p}^* monotonically increases with their size ℓ (figure 12). This is the case for the lattice with and without defects. Compact objects, such as triangles, have larger values of percolation thresholds than line segments and angled objects of the same length. Even low concentrations of impurities can prevent the formation of a percolating cluster. This can be seen from figure 12(b) where the results are shown for $p = 2\%$.

Blocking of the substrate area is enhanced with the growth of line segment length, making the surface more porous. This results in lower values of percolation thresholds. Porosity of the surface is also responsible for the low values of percolation thresholds in the case of angled objects for which there exists a greater probability for blocking the comprised sites so the percolation thresholds are even lower. Moreover, defects on

Figure 12. Dependence of the jamming coverage θ_{jam}, the percolation threshold θ_{p}^*, and the ratio $\theta_{\mathrm{p}}^*/\theta_{\mathrm{jam}}$ on the length ℓ of the walks placing triangles for two different concentrations of impurities: (a) $p = 0\%$, and (b) $p = 2\%$.
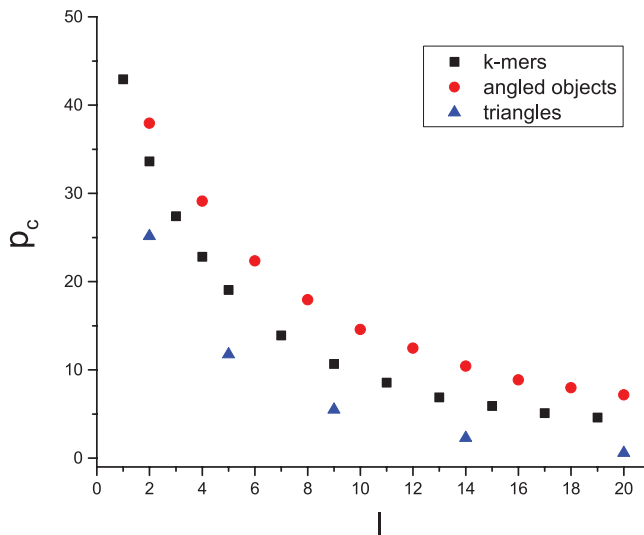
Figure 13. Dependence of the critical defect concentration p_c on the length ℓ of the objects for line segments (k-mers), angled objects and triangles. Objects and impurities are colored in white and red respectively.

a lattice are more successfully avoided by angled objects, which makes the percolation more robust in the presence of impurities. On the other hand, patterns formed by compact objects, such as triangles, are less porous and they give larger percolation thresholds.

Percolation is observed when the concentration of defects is smaller than a critical concentration of defects p_c. Figure 13 presents the critical defect concentrations p_c versus the length ℓ of the objects (see tables 2–4 for the numerical values). We can see the percolation can be reached at highest concentrations of impurities with angled objects. Triangles have the lowest values of critical concentrations and the worst performance regarding percolation.

5. Concluding remarks

We have investigated percolation and jamming phenomena for random sequential deposition of objects of various shapes and sizes on a 2D triangular lattice initially covered with point impurities at various concentrations p. The shapes are placed by self-avoiding lattice steps (see tables 1–4).

For each shape, it was shown that the exponential behavior (equation (1)) excellently describes the approach to the jamming limit θ_{jam} in the presence of defects. It was found that the rapidity of the approach to the jammed state is not affected by the presence of impurities. However, the corresponding jamming densities θ_{jam} decrease with the impurity concentration p. For small objects this dependence is linear up to very high impurity concentrations p, while for large objects coverage θ_{jam} decreases very rapidly with p. It was shown that the decay of the jamming limit θ_{jam} with the length of the walk ℓ placing the objects occurs via the exponential law (2) for all values of impurity concentration p. It was found that the characteristic length scale r (equation (2)) increases with p for low impurity concentrations, reaches a maximum, and decreases for higher values of p.

We have also presented numerical results for the irreversible deposition of multicomponent mixtures of objects from tables 2–4. In the case of polydisperse mixtures there is a significant difference in the behavior of partial jamming coverages for small and large component shapes when the concentration of impurities is increased. For small components of length $\ell = 1$ and $\ell = 2$, the partial jamming coverage grows with p for low impurity concentrations, reaches a maximum and decreases for larger concentrations of defects. This means that, at relatively low concentrations, partial coverage of the smallest object from the mixture can have even higher values than in the case of an initially clean lattice. On the other hand, the dependence of the partial jamming coverage is a monotonic function of impurity concentration p for larger components, $\ell > 2$.

It has been shown that, for k-mers and angled objects, the percolation threshold θ_{p}^* monotonically decreases with the size of the objects. However, in the case of more regular and compact shapes (triangles) the percolation threshold θ_{p}^* monotonically increases with the object size. In both cases, the percolation threshold θ_{p}^* is found to be practically insensitive to the point-like defect concentration. We have also shown that the ratio of percolation and jamming thresholds $\theta_{\mathrm{p}}^*/\theta_{\mathrm{jam}}$ increases with object size for all examined objects, regardless of the presence of impurities.

We have pointed out that for each object there is a concentration of defects p_c above which it is not possible to achieve percolation. For object arrangements made by the same number of steps the critical defect concentration has higher values for objects giving more porous surface configurations, and lower values for compact objects.

References

[1] Evans J W 1993 Random and cooperative sequential adsorption *Rev. Mod. Phys.* **65** 1281–329

[2] Privman V 2000 Dynamics of nonequilibrium deposition *Colloids Surf.* A **165** 231–40

[3] Talbot J, Tarjus G, Van Tassel P R and Viot P 2000 From car parking to protein adsorption: an overview of sequential adsorption processes *Colloids Surf.* A **165** 287–324

[4] Cadilhe A, Araújo N A M and Privman V 2007 Random sequential adsorption: from continuum to lattice and pre-patterned substrates *J. Phys.: Condens. Matter* **19** 065124

[5] Bartelt M C and Privman V 1991 Kinetics of irreverible adsorption of mixtures of pointlike and fixed-size particles: exact results *Phys. Rev.* A **44** R2227–30

[6] Ben-Naim E and Krapivsky P L 1994 On irreversible deposition on disordered substrates *J. Phys. A: Math. Gen.* **27** 3575

[7] Fan Y and Percus J K 1992 Random sequential adsorption on a ladder *J. Stat. Phys.* **66** 263–71

[8] Baram A and Kutasov D 1994 Random sequential adsorption on a 3∗ infinity lattice: an exact solution *J. Phys. A: Math. Gen.* **27** 3683

[9] Cieśla M 2013 Continuum random sequential adsorption of polymer on a flat and homogeneous surface *Phys. Rev.* E **87** 052401

[10] Cieśla M and Barbasz J 2014 Kinetics of random sequential adsorption of nearly spherically symmetric particles *Phys. Rev.* E **89** 022401

[11] Cieśla M and Barbasz J 2014 Random packing of regular polygons and star polygons on a flat two-dimensional surface *Phys. Rev.* E **90** 022402

[12] Cieśla M and Karbowniczek P 2015 Random sequential adsorption of starlike particles *Phys. Rev.* E **91** 042404

[13] Manna S S and Švrakić N M 1991 Random sequential adsorption: line segments on the square lattice *J. Phys. A: Math. Gen.* **24** L671–6

[14] Cornette V, Linares D, Ramirez-Pastor A J and Nieto F 2007 Random sequential adsorption of polyatomic species *J. Phys. A: Math. Theor.* **40** 11765–76

[15] Erban R and Chapman S J 2007 On chemisorption of polymers to solid surfaces *J. Stat. Phys.* **127** 1255–77

[16] Budinski-Petković Lj and Kozmidis-Luburić U 1997 Random sequential adsorption on a triangular lattice *Phys. Rev.* E **56** 6904

[17] Budinski-Petković Lj, Vrhovac S B and Lončarević I 2008 Random sequential adsorption of polydisperse mixtures on discrete substrates *Phys. Rev.* E **78** 061603

[18] Budinski-Petković Lj, Lončarević I, Jakšić Z M, Vrhovac S B and Švrakić N M 2011 Simulation study of anisotropic random sequential adsorption of extended objects on a triangular lattice *Phys. Rev.* E **84** 051601

[19] Švrakić N M and Henkel M 1991 Kinetics of irreversible deposition of mixtures *J. Phys.* I **1** 791–5

[20] Meakin P and Jullien R 1992 Random-sequential adsorption of disks of different sizes *Phys. Rev.* A **46** 2029

[21] Lončarević I, Budinski-Petković Lj and Vrhovac S B 2007 Simulation study of random sequential adsorption of mixtures on a triangular lattice *Eur. Phys. J.* E **24** 19–26

[22] Brilliantov N V, Andrienko Yu A, Krapivsky P L and Kurths J 1996 Fractal formation and ordering in random sequential adsorption *Phys. Rev. Lett.* **76** 4058

[23] Adamczyk Z, Siwek B, Zembala M and Weroński P 1997 Influence of polydispersity on random sequential adsorption of spherical particles *J. Colloid Interface Sci.* **185** 236–44

[24] Staufer D and Aharony A 1994 *Introduction to Percolation Theory* (London: Taylor and Francis)

[25] Sahimi M 1994 *Applications of Percolation Theory* (London: Taylor and Francis)

[26] Newman M E J and Watts D J 1999 Scaling and percolation in the small-world network model *Phys. Rev.* E **60** 7332–42

[27] Kondrat G and Pękalski A 2001 Percolation and jamming in random sequential adsorption of linear segments on a square lattice *Phys. Rev.* E **63** 051108

[28] Rampf F and Albano E V 2002 Interplay between jamming and percolation upon random sequential adsorption of competing dimers and monomers *Phys. Rev.* E **66** 061106

[29] Kondrat G 2002 Influence of temperature on percolation in a simple model of flexible chains adsorption *J. Chem. Phys.* **117** 6662

[30] Kondrat G 2008 Impact of composition of extended objects on percolation on a lattice *Phys. Rev.* E **78** 011101

[31] Restrepo J G, Ott E and Hunt B R 2008 Weighted percolation on directed networks *Phys. Rev. Lett.* **100** 058701

[32] Tsakiris N, Maragakis M, Kosmidis K and Argyrakis P 2010 Percolation of randomly distributed growing clusters: finite-size scaling and critical exponents for the square lattice *Phys. Rev.* E **82** 041108

[33] Cherkasova V A, Tarasevich Y Y, Lebovka N I and Vygornitskii N V 2010 Percolation of aligned dimers on a square lattice *Eur. Phys. J.* B **74** 205–9

[34] Ziff R M 2009 Explosive growth in biased dynamic percolation on two-dimensional regular lattice networks *Phys. Rev. Lett.* **103** 045701

[35] Ioselevich A S and Kornyshev A A 2002 Approximate symmetry laws for percolation in complex systems: percolation in polydisperse composites *Phys. Rev.* E **65** 021301

[36] Araújo N A M and Herrmann H J 2010 Explosive percolation via control of the largest cluster *Phys. Rev. Lett.* **105** 035701

[37] Lebovka N I, Karmazina N N, Tarasevich Y Yu and Laptev V V 2011 Random sequential adsorption of partially oriented linear *k*-mers on a square lattice *Phys. Rev.* E **84** 061603

[38] Cohen R, Erez K, Ben Avraham D and Havlin S 2001 Breakdown of the internet under intentional attack *Phys. Rev. Lett.* **86** 3682–5

[39] Adamczyk P, Romiszowski P and Sikorski A 2008 A simple model of stiff and flexible polymer chain adsorption: the influence of the internal chain architecture *J. Chem. Phys.* **128** 154911

[40] Budinski-Petković Lj, Lončarević I, Petković M, Jakšić Z M and Vrhovac S B 2012 Percolation in random sequential adsorption of extended objects on a triangular lattice *Phys. Rev.* E **85** 061117

[41] Porto M and Eduardo Roman H 2000 Critical packing fraction of rectangular particles on the square lattice *Phys. Rev.* E **62** 100–2

[42] Nakamura M 1987 Percolational and fractal property of random sequential packing patterns in square cellular structures *Phys. Rev.* A **36** 2384–8

[43] Cornette V, Ramirez-Pastor A J and Nieto F 2006 Percolation of polyatomic species on site diluted lattices *Phys. Lett.* A **353** 452–8

[44] Centres P M and Ramirez-Pastor A J 2015 Percolation and jamming in random sequential adsorption of linear *k*-mers on square lattices with the presence of impurities *J. Stat. Mech.* P10011

[45] Tarasevich Y Yu, Laptev V V, Vygornitskii N V and Lebovka N I 2015 Impact of defects on percolation in random sequential adsorption of linear *k*-mers on square lattices *Phys. Rev.* E **91** 012109

[46] Newman M E J and Ziff R M 2000 Efficient Monte Carlo algorithm and high-precision results for percolation *Phys. Rev. Lett.* **85** 4104–7

[47] Newman M E J and Ziff R M 2001 Fast Monte Carlo algorithm for site or bond percolation *Phys. Rev.* E **64** 016706